

HOSSnet: an Efficient Physics-Guided Neural Network for Simulating Crack Propagation

Shengyu Chen^{a,b,*}, Shihang Feng^{a,*}, Yao Huang^a, Zhou Lei^a, Xiaowei Jia^b, Youzuo Lin^a, Estaben Rougier^a

^aEarth and Environmental Science Division, Los Alamos National Laboratory, Los Alamos, NM 87545, USA

^bDepartment of Computer Science, University of Pittsburgh, Pittsburgh, PA, 15260

ARTICLE INFO

Article history:

Received 1 May 2023

Received in final form 10 May 2023

Accepted 13 May 2023

Available online 15 May 2023

Communicated by XXX

ABSTRACT

Hybrid Optimization Software Suite (HOSS), which is a combined finite-discrete element method (FDEM), is one of the advanced approaches to simulating high-fidelity fracture and fragmentation processes but the application of pure HOSS simulation is computationally expensive. At the same time, machine learning methods, shown tremendous success in several scientific problems, are increasingly being considered promising alternatives to physics-based models in the scientific domains. Thus, our goal in this work is to build a new data-driven methodology to reconstruct the crack fracture accurately in the spatial and temporal fields. We leverage physical constraints to regularize the fracture propagation in the long-term reconstruction. In addition, we introduce perceptual loss and several extra pure machine learning optimization approaches to improve the reconstruction performance of fracture data further. We demonstrate the effectiveness of our proposed method through both extrapolation and interpolation experiments. The results confirm that our proposed method can reconstruct high-fidelity fracture data over space and time in terms of pixel-wise reconstruction error and structural similarity. Visual comparisons also show promising results in long-term reconstruction.

© 2023 Elsevier Inc. All rights reserved.

1. Introduction

Knowledge of brittle materials failure is significant since they have been widely applied in a variety of areas, including structural engineering, geotechnical engineering, mechanical engineering, geothermal engineering, and the oil & gas industry. The mechanism of brittle material failure is strongly affected by the microstructure of the material, especially the pre-existing micro cracks [1, 2]. The dynamic propagation and interaction behavior of micro-cracks is

*This is an example for title footnote coding.

*Corresponding author

essential to estimate the failure of brittle material [3, 4]. The growth and coalescence of micro-cracks will result in a complex stress state near the crack tips, leading to the catastrophic failure of brittle material in macro-scale [5, 6].

Many approaches have been proposed in the literature to analyze the crack initiation, and propagation behavior in brittle materials, including theoretical constitutive models and numerical methods [7, 8, 9, 10, 11, 12, 13, 14, 15, 16]. The finite-discrete element method (FDEM) is one of the advanced approaches [17]. Based on the FDEM, the Hybrid Optimization Software Suite (HOSS) [18] is developed as a fracture simulator. This high-fidelity model simulates fracture and fragmentation processes or materials deformation in both 2D and 3D complex systems, providing accurate predictions of fracture growth and material failure. However, the application of pure HOSS simulation has computational limitations since they resolve all the individual cracks with highly resolved meshes and small time steps at large scales. Hence, a new approach can provide key quantities of interest with more efficiency but retain reasonable accuracy in demand.

Machine learning (ML) models are gaining significant attention as a promising alternative to physical simulations in recent years due to their remarkable success and high efficiency in various applications, such as image segmentation [19, 20, 21] and image reconstruction [22, 23, 24]. Encoder-decoder networks [25] have been employed to simulate the intricate two-dimensional subsurface fluid dynamics occurring in porous media [26]. Fourier Neural Operator [27], which combines Fourier analysis and neural networks, has been utilized to solve complex physical problems, such as wave propagation [28] and multiphase flow dynamics [29]. Temporal models, such as the long short-term memory (LSTM) model, have been extensively utilized to capture long-term dependencies in temporal propagation. For instance, in the hydrology domain, the LSTM model has been broadly used to model temporal patterns of water dynamics [30, 31].

To speed up the simulation of HOSS, ML approaches had been utilized to emulate the high-fidelity model efficiently. The micro-cracks are represented by a feature vector, then a variety of ML methods, such as decision trees, random forest, and artificial neural networks, are utilized to predict the time and the location of fracture coalescence [32, 33, 34]. But the fracture damage, which is the key input needed for upscaling micro-scale information to macro-scale models, is not estimated. A graph convolutional network (GCNs), coupled with a recurrent neural network (RNN), was used to model the evolution of those features from the reduced graph representation of large fracture networks [35], where the sum of the fracture damage in each finite element mesh is represented as total damage. However, these works only consider using the fracture features to predict its propagation.

In this paper, we develop a new data-driven method, termed Hybrid Optimization Software Suite Network (HOSSnet), to improve the high-fidelity of micro-crack fracture reconstruction from Cauchy stress and fracture damage in spatial and temporal fields. We also leverage the underlying physical constraints to further regularize the model learning of generalizable spatial and temporal patterns in the reconstruction process. In particular, our proposed method consists of two components: high-fidelity reconstruction unit (HRU) and physics-guided regularization. HRU is designed based on an Unet-based [36] encoder-decoder structure to improve the reconstruction performance in the spatial field. HRU also uses an LSTM layer to capture long-term temporal dependencies. In addition, The physics-guided regularization method adjusts the reconstructed data over time by enforcing consistency with known physical constraints such as optical flow [37] and positive direction.

Our evaluations of the HOSS dataset [18] have shown the promising performance of the proposed HOSSnet over space and time in both interpolation and extrapolation experiments. We also demonstrate the effectiveness of each component of our design by showing the improvement both qualitatively and quantitatively.

2. Related Work

2.1. Machine Learning Approaches in Scientific Domain

Machine learning (ML) models, given their tremendous success in several commercial applications (e.g., computer vision, natural language processing, etc.), are increasingly being considered promising alternatives to physics-based models in the scientific domains. For example, in the hydrology domain, researchers have used graph neural networks (GNN) in modeling spatial dependencies [38, 39] of river networks. In streamflow problems, Moshe et al. [38] proposed the HydroNets model, which uses ML models to integrate the information from river segments and their upstream segments to improve the streamflow predictions. Chen et al. [39] proposed a Heterogeneous Stream-reservoir Graph Network (HRGN) model to represent underlying stream-reservoir networks and improve streamflow temperature prediction in all river segments within a river network.

The convolutional neural network (CNN) based and generative adversarial networks (GAN) based models have been widely used in high-resolution turbulent flow simulation. Fukami et al. [40] propose an improved CNN-based hybrid downsampled skip-connection/multi-scale (DSC/MS) model by extracting patterns from multiple scales. This method has been shown to produce a good performance in reconstructing the turbulent velocity and vorticity fields from extremely low-resolution input data. Similarly, Liu et al. [41] also propose another CNN-based multiple temporal paths convolutional neural network (MTPC) to simultaneously handle spatial and temporal information in turbulent flow simultaneously to fully capture features in different time ranges. Deng et al. [42] demonstrate that both super-resolution generative adversarial networks (SRGAN) and enhanced super-resolution generative adversarial networks (ESRGAN) [43] can produce a reasonable reconstruction of high-resolution turbulent flow in their datasets.

In the micro-crack problem, Perera [44] proposed a graph neural network to represent the relationship of different cracks and initially realize simulating cracks propagation for a wide range of initial microcrack configurations. This method only considers the cracks propagation from fracture features to fracture features but cannot apply to the model mapping from Cauchy features to fracture features.

2.2. Physics-based Loss Function

There are still several challenges faced by existing machine learning methods. Standard machine learning models can fail to capture complex relationships amongst physical variables. Results will be even worse if only contain limited observation data. This is one reason for their failure to generalize to scenarios not encountered in training data. Hence, researchers are beginning to incorporate physical knowledge into loss functions to help machine learning models capture generalizable dynamic patterns consistent with established physical relationships. In recent studies [45, 46], the use of physical-based loss functions has already shown promising results in a variety of scientific disciplines. For example, Karpatne et al. [47] propose an additional physics-based penalty based on known monotonic physical relationship to guarantee that the density of water at lower depth is always greater than the density of water in any depths above. Kahana et al. [48] apply an additional loss function to ensure the physical consistency in the time evolution of waves, improving the prediction results and making the model more robust.

3. Problem Definition

The objective of our proposed work is to reconstruct the missing fracture image \mathbf{Y} for each micro-crack $m \in \{1, \dots, M\}$ at each time step $t \in \{1, \dots, T\}$, given input physical variables that drive the dynamics of the physical system. In detail, we use $\mathbf{X}_c = \{\mathbf{x}_{m,c}^t\}$ to represent dynamic Cauchy input features for each micro-crack m at a specific time step t . \mathbf{X}_c includes three Cauchy features of all micro-crack: Cauchy1 C_x , Cauchy2 C_y , and Cauchy12 C_{xy} . In another case, we also regard $\mathbf{X}_f = \{\mathbf{x}_{m,f}^t\}$ as a dynamic fracture input feature for each micro-crack on each time step. Then we use these two different groups of input features: \mathbf{X}_c and \mathbf{X}_f to reconstruct the missing target variables (i.e., fracture) $\mathbf{Y} = \{y_m^t\}$ for certain micro-crack on certain time step respectively. When \mathbf{X}_c is used as the input, we represent this scenario as Cauchy \rightarrow Fracture. On the contrary, the scenario would be Fracture \rightarrow Fracture if \mathbf{X}_f is the input.

4. Methods

The purpose of our proposed HOSSnet model is used to achieve an end-to-end reconstruction mechanism from input feature \mathbf{X} (Cauchy feature \mathbf{X}_c or fracture feature \mathbf{X}_f) to missing target variable (i.e., fracture) \mathbf{Y} over the time and over the sample. In Figure.1. we show the overall structure of the proposed HOSSnet method. These are described here, in order:

4.1. HOSSnet Architecture

This proposed HOSSnet aims to learn the model mapping from \mathbf{X} to \mathbf{Y} , containing two main components: HRU and physics-guided regularization.

HRU is designed based on benchmark Unet-based [36] encoder-decoder structure. It contains a contracting path (encoder), recurrent network layer (RTL), and expansive path (decoder). The contracting path consists of the repeated application of two 3x3 convolutions (unpadded convolutions), each followed by a rectified linear unit (ReLU) [49] and a 2x2 max pooling operation with stride 2 for downsampling. Additionally, we also introduce multiple residual blocks between every two convolutions. And each residual block contains convolutional layers [50], batch normalization

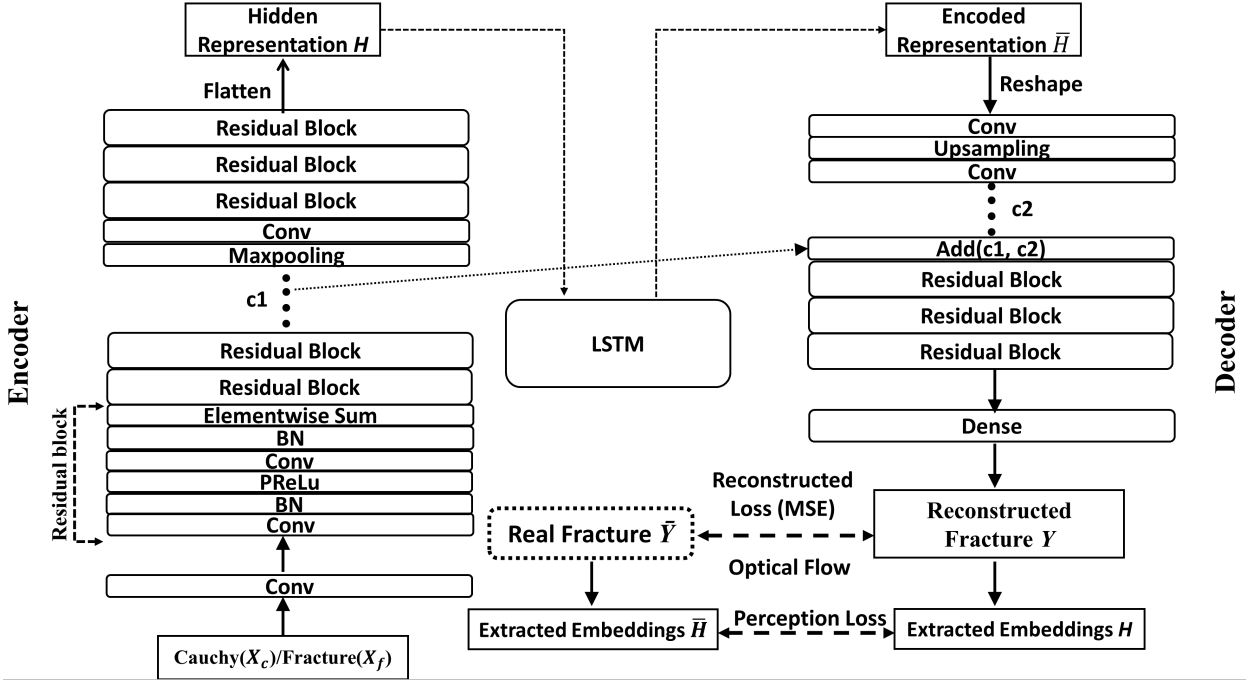


Fig. 1: The architecture of the proposed HOSSnet model and different components in the loss function.

layers [51], and parametric ReLUs following previous literature [52]. We feed the input feature \mathbf{X} into this encoder and encode the \mathbf{X} into a series of hidden representations $\mathbf{H} = \{h_m^t\}$ for certain micro-crack on certain time steps respectively. After extracting the hidden representations $\mathbf{H} = \{h_m^t\}$, we feed them into the recurrent transition layer (RTL), which is built based on LSTM structure [53]. We obtain the new hidden representation $\hat{\mathbf{H}} = \{\hat{h}_m^t\}$ in this RTL structure. Lastly, we continue to move the obtained $\hat{\mathbf{H}}$ to the expansive path (decoder) for outputting reconstructed fracture data \mathbf{Y} . In particular, the expansive path consists of an upsampling of the feature map followed by a 2×2 convolution (“up-convolution”) that halves the number of feature channels, a concatenation with the correspondingly cropped feature map from the contracting path, and two 3×3 convolutions, each followed by a ReLU activation. The overall framework details are shown in Table. 1.

The HOSSnet model outputs a reconstructed fracture data \mathbf{Y} , the model is optimized to reduce the difference between obtained $\mathbf{Y} = \{y_m^t\}$ and provided ground truth fracture data $\hat{\mathbf{Y}} = \{\hat{y}_m^t\}$ for certain micro-crack m on certain time step t . Such a difference is represented as a loss $\mathcal{L}_{\text{MSE}}(\mathbf{Y}, \hat{\mathbf{Y}})$, which can be implemented as mean squared loss (MSE) that measure the difference between two sets of data. The loss function can be represented as

$$\mathcal{L}_{\text{MSE}}(\mathbf{Y}, \hat{\mathbf{Y}}) = \frac{1}{|\mathbf{Y}|} \sum_{\{(m,t)|y_m^t \in \mathbf{Y}\}} (y_m^t - \hat{y}_m^t)^2 \quad (1)$$

4.2. Physics-Guided Regularization

We further regularize our proposed model by leveraging the physical knowledge: optical flow [54] and positive direction to optimize the reconstruction performance by several approaches described below.

4.2.1. Optical Flow

Optical flow has been used as a method to describe the movement of an object between consecutive frames of the images [54], and we adopt it to represent the development of the fracture \mathbf{Y} . At each pixel location, the optical flow vector represents the motions of the pixel from one frame to another. Specifically, we consider each pixel in the fracture image $\mathbf{Y}(x, y, t)$ moving to $\mathbf{Y}(x + \Delta x, y + \Delta y, t + \Delta t)$ after the time interval Δt . If the movements is small, $\mathbf{Y}(x + \Delta x, y + \Delta y, t + \Delta t)$ can be expanded using a Tayler series:

$$\mathbf{Y}(x + \Delta x, y + \Delta y, t + \Delta t) = \mathbf{Y}(x, y, t) + \mathbf{Y}_x \Delta x + \mathbf{Y}_y \Delta y + \mathbf{Y}_t \Delta t + \dots, \quad (2)$$

where \mathbf{Y}_x , \mathbf{Y}_y and \mathbf{Y}_t are partial derivative with respect to x , y and t . If we consider the target pixel to be the same before and after the movement, we have $\mathbf{Y}(x + \Delta x, y + \Delta y, t + \Delta t) = \mathbf{Y}(x, y, t)$. Combining with Eq. (2) by ignoring the higher order terms (i.e., "..."), we have

$$\mathbf{Y}_x u + \mathbf{Y}_y v + \mathbf{Y}_t = 0, \quad (3)$$

where u and v are the x and y components of the motion vector $\mathbf{m} = (u, v)$, which is defined as

$$u = \frac{\Delta x}{\Delta t}, v = \frac{\Delta y}{\Delta t}. \quad (4)$$

The motion vector $\mathbf{m} = (u, v)$ can be obtained by minimizing the objective function with a smooth regularization,

$$\zeta^{\text{op}} = \iint \left((\mathbf{Y}_x u + \mathbf{Y}_y v + \mathbf{Y}_t)^2 + \lambda^2 M^2 \right) dx dy, \quad (5)$$

where λ is the weight for the smoothing regularization, and M is the magnitude of the flow gradient given by

$$M(u, v) = \sqrt{\|\nabla u\|^2 + \|\nabla v\|^2}. \quad (6)$$

In this paper, we calculate the observed optical flow vector $\mathbf{m}_1 = (u_1, v_1)$ from the observed fractures $\hat{\mathbf{Y}}$ and the predicted optical flow vector $\mathbf{m}_2 = (u_2, v_2)$ from the predicted fractures \mathbf{Y} . Then we use the included angle between these two vectors as the regularization in the optical loss function \mathcal{L}_{op} , which can be described as

$$\mathcal{L}_{\text{op}} = \sum_n \|\arccos(r_n(u_1, u_2, v_1, v_2))\|^2, \quad (7)$$

where the operator $\arccos(\cdot)$ is the inverse of the cosine function. The function of $r_n(u_1, u_2, v_1, v_2)$ is defined as

$$r_n(u_1, u_2, v_1, v_2) = \frac{u_1 u_2 + v_1 v_2}{\sqrt{u_1^2 + v_1^2} \sqrt{u_2^2 + v_2^2}}, \quad (8)$$

Thus, the overall loss function for the extrapolation network with optical flow regularization can be posed as

$$\mathcal{L}_{\text{MSE}_{\text{op}}} = \mathcal{L}_{\text{MSE}} + \alpha_{\text{op}} \mathcal{L}_{\text{op}}, \quad (9)$$

where the terms of \mathcal{L}_{MSE} and \mathcal{L}_{op} are provided in Eqs. (10) and (7), respectively, and α_{op} is the weight for the regularization term. The regularization term would constrain the direction of the fracture development.

4.2.2. Positive Direction

Ideally, the fracture development should always be positive with time changes. Without the awareness of such development patterns, the neural network model can still output negative changes. In order to force the fracture to develop in a positive direction, we have eliminated the negative change points during the prediction stage and set these points the same as the previous time step.

4.3. Machine Learning Optimization Approaches

4.3.1. Perceptual Loss

In order to further improve the reconstruction performance, we not only use the content loss based on MSE but also introduce the perceptual loss calculated based on the feature map of the VGG network [55], which works by summing all the squared errors between all the pixels and taking the mean. This is in contrast to a pixel-wise loss function (e.g., MSE) which sums all the absolute errors between pixels. This perceptual loss $\mathcal{L}_{\text{Perceptual}}$ can be represented as:

$$\mathcal{L}_{\text{Perceptual}}(\mathbf{E}, \hat{\mathbf{E}}) = \frac{1}{|\mathbf{E}|} \sum_{\{(m,t)|e'_m \in \mathbf{E}\}} (v'_m - \hat{e}'_m)^2, \quad (10)$$

where \mathbf{E} and $\hat{\mathbf{E}}$ represent the pixel features extracted from VGG network for \mathbf{Y} and $\hat{\mathbf{Y}}$ respectively. Hence, the loss function $\mathcal{L}_{\text{recon}}$ can be replaced by

$$\mathcal{L}_{\text{recon}}(\mathbf{Y}, \hat{\mathbf{Y}}) = \mathcal{L}_{\text{MSE}}(\mathbf{Y}, \hat{\mathbf{Y}}) + \alpha_{\text{perc}} \mathcal{L}_{\text{Perceptual}}(\mathbf{Y}, \hat{\mathbf{Y}}), \quad (11)$$

where α_{perc} is the weight of perceptual loss. Overall, after adding all the regularization and physical information, the loss function for the optimization will be

$$\mathcal{L}_{\text{all}}(\mathbf{Y}, \hat{\mathbf{Y}}) = \mathcal{L}_{\text{MSE}}(\mathbf{Y}, \hat{\mathbf{Y}}) + \alpha_{\text{perc}} \mathcal{L}_{\text{Perceptual}}(\mathbf{Y}, \hat{\mathbf{Y}}) + \alpha_{\text{op}} \mathcal{L}_{\text{op}}(\mathbf{Y}, \hat{\mathbf{Y}}). \quad (12)$$

Table 1: The detailed parameters' information of overall HOSSnet Framework including encoder(upper), recurrent transition model(middle), and decoder(lower).

Layers	Filter Size	State size
Convolutional layer	(3, 3)	64
Residual Block	(3, 3)	64
Residual Block	(3, 3)	64
Residual Block	(3, 3)	64
Maxpooling	None	None
Convolutional layer	(3, 3)	64
Residual Block	(3, 3)	64
Residual Block	(3, 3)	64
Residual Block	(3, 3)	64
Convolutional layer	(3, 3)	64
LSTM Layer	None	64
Convolutional layer	(3, 3)	64
Upsampling	None	None
Add	None	None
Residual Block	(3, 3)	64
Residual Block	(3, 3)	64
Residual Block	(3, 3)	64
Convolutional layer	(3, 3)	64
Fully-Connection layer	None	None

4.3.2. Sub-region

In addition, when we utilize the extrapolation and the interpolation task, we know the location of the fracture from the known data. Instead of training with the whole image, we train the network with the sub-region of the images \mathbf{Y}_{sub} containing the fracture dynamic. This is because the most of region of the whole image has no change, making the built HOSSnet model less sensitive to the sub-region containing fracture dynamic. Hence, the loss function after adding this optimization will be replaced as:

$$\mathcal{L}_{all}(\mathbf{Y}_{sub}, \hat{\mathbf{Y}}_{sub}) = \mathcal{L}_{MSE}(\mathbf{Y}_{sub}, \hat{\mathbf{Y}}_{sub}) + \alpha_{Perc} \mathcal{L}_{Perceptual}(\mathbf{Y}_{sub}, \hat{\mathbf{Y}}_{sub}) + \alpha_{op} \mathcal{L}_{op}(\mathbf{Y}_{sub}, \hat{\mathbf{Y}}_{sub}). \quad (13)$$

5. Experiment

This section will first describe the HOSS dataset and the experiment settings. Then we evaluate the performance of our proposed methods for fracture reconstruction.

5.1. Experiment Setting

We consider two experiments: Extrapolation and Interpolation. The former is designed to verify the ability of the proposed method to reconstruct micro-crack fractures in the future state. We have conducted experiments over the sample, in which the test is performed on different samples from the training set. In addition, The experiments over time are performed, wherein predictions were made on the same sample, but across different time periods from the training set. The latter is designed to verify the ability of the proposed method to reconstruct micro-crack fracture in the intermediate time period.

5.1.1. Dataset

The high-fidelity HOSS simulator has been applied to simulate the fracture growth and material failure of a concrete sample under uniaxial tensile loading conditions. Then, the generated simulation data are converted to images by ParaView for the training of HossNet. The problem is considered a 2D problem, and the model setup is shown in Figure 2. The domain is a rectangular sample 2m wide and 3m high. The bottom edge of the sample is fixed. The top edge of the sample moves upwards with a constant velocity of 0.3m/s, which results in a strain rate of $0.1s^{-1}$. The material is assumed to be elastically isotropic for all cases with the elastic material properties: 2500kg/m³ for density, 22.6 GPa for Young's modulus, and 0.242 for Poisson's ratio.

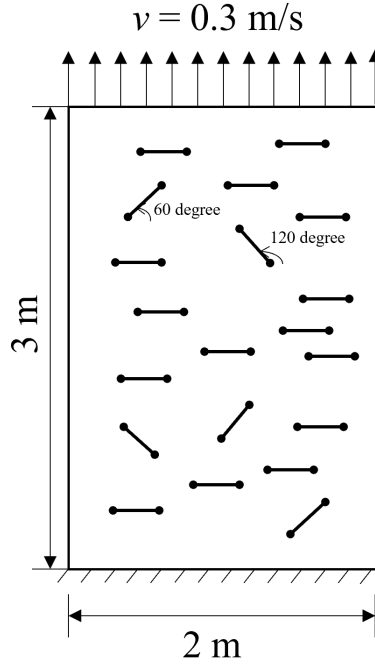


Fig. 2: Model setup for the 2D uni-axial tensile failure problem with 20 pre-existing cracks.

5.1.2. Evaluation Metrics

We evaluate the performance of micro-reconstruction using three different metrics, root mean squared error (RMSE), structural similarity index measure (SSIM) [56], and weighted fracture error (WFE). We use RMSE to measure the difference (error) between reconstructed data and target fracture data. The lower value of RMSE indicates better reconstruction performance. SSIM is used to appraise the similarity between reconstructed data and target fracture on three aspects, luminance, contrast, and overall structure. The higher value of SSIM indicates better reconstruction performance. Lastly, we also create a new evaluation metric: weighted local fracture error (WFE), to measure the difference by using mean squared error, given the higher weight of the local region with dynamic change of micro-crack fracture. This evaluation metric can be represented as:

$$\text{WFE} = 10\text{RMSE}(\mathbf{Y}_{dym} - \hat{\mathbf{Y}}_{dym}) + \text{RMSE}(\mathbf{Y}_{fix} - \hat{\mathbf{Y}}_{fix}), \quad (14)$$

where \mathbf{Y}_{dym} and \mathbf{Y}_{fix} denote the dynamic region and fixed region, respectively. The local crack prediction performance is more effectively represented by the WFE metric as compared to RMSE due to its emphasis on the local region. Similar to RMSE, the lower value of WFE indicates better reconstruction performance as well.

5.1.3. Baselines

We compare the performance of the proposed HOSSnet method against several existing methods that have been widely used for data reconstruction. Specifically, we implement the HRU, and CNN-LSTM as baselines. To better verify the effectiveness of each component in our proposed method, we further compared HOSSnet with its variants: HOSSnet-F, which removes the perception loss from the complete model and only includes physical regularization in the proposed method. Additionally, by comparing HOSSnet-F and CNN-LSTM, we show improvement by incorporating physical regularization. We can further verify the effectiveness of the perception loss by comparing HOSSnet-F and HOSSnet.

5.1.4. Experimental Design

We evaluate the performance of our proposed method in two different scenarios.

First, we conduct the extrapolation experiment, which includes over-time and over-sample tests, to study how the proposed HOSSnet method helps simulate fracture change in both over-time and over-sample situations. Specifically, in the over-time test, we select 6 different cracks in our test. We use the 5 complete crack samples and the first 150 time steps of the sixth crack sample as training and reconstruct the crack data in the remaining 150-time steps. In the

Table 2: Average reconstruction performance (measured by RMSE, SSIM, and WFE) of first 50th time steps in Cauchy \rightarrow Fracture’s experiment on extrapolating over the sample (upper), extrapolating over time (middle), interpolating (lower) respectively.

Experiment	Method	RMSE \downarrow	SSIM \uparrow	WFE \downarrow
Over Sample	HRU	0.057	0.965	0.091
	CNN-LSTM	0.046	0.971	0.083
	HOSSnet-F	0.038	0.979	0.077
	HOSSnet	0.028	0.982	0.060
Over Time	HRU	0.023	0.985	0.061
	CNN-LSTM	0.018	0.985	0.052
	HOSSnet-F	0.011	0.991	0.034
	HOSSnet	0.009	0.995	0.024
Interpolation	HRU	0.025	0.985	0.057
	CNN-LSTM	0.020	0.987	0.046
	HOSSnet-F	0.018	0.988	0.049
	HOSSnet	0.014	0.991	0.036

over-sample test, we also use 6 different crack samples, each sample containing 300-time steps crack data. We use the 5 different crack samples as training and reconstruct the complete sequence of the remaining crack sample. Both over-time and over-sample tests are challenging tasks since micro-crack fracture is changing over time following complex non-linear patterns (driven by a partial differential equation). Hence, in the over-time test, the model trained from available data may not be able to generalize to future data that look very different from training data. Furthermore, it is more difficult to achieve the complete sequence of data reconstruction in the over-sample test because the model cannot capture any pattern of the testing data.

Second, we consider the case in which the intermediate time period of data is missing. For example, the fracture data is available at the beginning and end time periods but missing in the intermediate time steps. We can use the model trained using available data (beginning and ending) to reconstruct the fracture data in the missing time steps.

We refer to this test as an interpolation experiment. In this test, we use the single crack sample in our test, containing 300 available time steps. In the first case, we divide the data into 3 parts and each part has 100-time steps of data. We use the first and last 100 time steps as training and use the remaining intermediate 100-time steps for testing. In the other case, we only use 10% time steps as the training set, which we include the dataset into the training set every 10-time steps, the remaining are the test set.

5.1.5. Training Settings

Data normalization is performed on both training and testing datasets, to normalize input variables to the range [0, 1]. Then, the model is trained by ADAM optimizer [57] The initial learning rate is set to 0.0005 and iterations are 500 epochs. We use Tensorflow 2.6 and Keras to implement our models with V100 GPU.

5.2. Cauchy 1, 12, 2 \rightarrow Fracture

This section shows the experimental results of Cauchy features \rightarrow Fracture, which also includes extrapolating over the sample, over time, and interpolating experiments.

5.2.1. Extrapolation Over Sample

Quantitative Results. The upper section of Table. 2, shows quantitative comparisons amongst all the methods, including average RMSE, SSIM, and WFE in the first 50-time steps of the testing phase. When comparing our proposed HOSSnet method with baseline methods. our proposed HOSSnet performs the best in three evaluation ways: obtain the lowest RMSE and WFE values, and the highest SSIM values. According to this table, the proposed method HOSSnet, in general, outperforms other baselines in terms of three different evaluation metrics. By comparing HRU and CNN-LSTM, we show the improvement by using the RTL structure. Furthermore, the comparison amongst CNN-LSTM, HOSSnet-F, and HOSSnet shows the effectiveness of incorporating the physics-guided regularization method (optical flow and perpetual loss) of the proposed method. In particular, the incorporation of perpetual loss brings the most significant performance improvement in terms of RMSE, SSIM, and WFE values.

Temporal Analysis In the temporal analysis, we show the change in performance as we reconstruct fracture data over 60-time steps after the training data. We show the performance of long-term prediction in terms of RMSE and WFE in Figures. 3. Several observations are highlighted: (1) With larger time intervals between training data

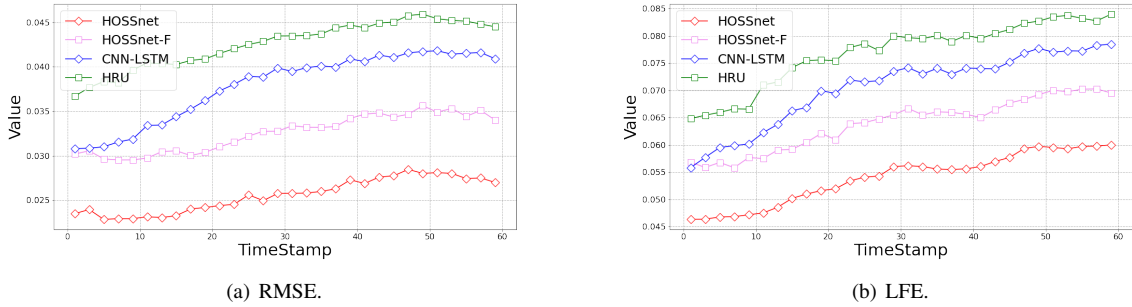


Fig. 3: Change of RMSE and WFE values produced by different models from the 1st to the 60th time (interval is 2 time steps) step in the extrapolating over sample experiment.

and prediction data, the performance becomes worse. In general, our proposed HOSSnet method outperforms other baselines. (2) We can obtain a similar conclusion by comparing HRU and CNN-LSTM. The proposed RTL component can bring significant improvement in long-term propagation. (3) We also can justify the effectiveness of the proposed physics-guided regularization method and extra perpetual loss by comparison amongst CNN-LSTM, HOSSnet-F, and HOSSnet.

Visual Results. Figures. 4 shows the reconstructed fracture at multiple time steps (50th, 60th, 70th, 80th, and 90th-time steps) after the training period. For each time step, we show the images from ground truth and the HOSSnet method. In the first few time steps, we can observe that our proposed HOSSnet can obtain ideal visual results. The performance is very similar to the ground truth image. After several time steps (e.g., 70th-time step), we can find the reconstruction performance is become slightly worse than the ground truth image but still can effectively fine-level captures textures and patterns, and obtain reasonable performance, only containing a slight blur in the sub-region of the dynamic of fracture. It also proves the effectiveness of the proposed HOSSnet method in long-term reconstruction.

5.2.2. Extrapolation Over Time

Quantitative Results. In this experiment, we compare the same set of existing methods as in the previous Extrapolation Over Sample experiment. In the middle part section of Table 2, we show the quantitative results of the first 50-time steps in the testing set. We can observe similar results that our proposed HOSSnet outperforms other methods by a considerable margin. We still can notice a significant improvement by adding each component: RTL, Physics-Guided Regularization, and perpetual loss, but the degree of improvement is not as high as in the over-sample experiments. This is because we also use the first 150-time steps of testing crack data as training except for 5 complete sequences of crack data. This is very helpful for the ML model to capture the initial complex pattern and dynamic transformation of the testing data. In such a case, a simple HRU model can get a relatively reasonable result. Therefore, the improvement brought by adding other components later will not be as obvious as in the previous over-sample experiment.

We also show the details of temporal analysis and visual results for this extrapolating over-time experiment in the supplementary file. We almost can obtain a similar conclusion as the experiment of extrapolating over the sample. Our proposed method can achieve promising reconstruction performance in long-term propagation.

5.2.3. Interpolation

Quantitative Results. In this single crack experiment, we compare the same set of existing methods as in the previous two extrapolating experiments. In the lower part section of Table 2, we show the quantitative results including average RMSE, SSIM, and WFE in the first 50 time steps of the testing set. From the table, we also obtain the same conclusion that our proposed HOSSnet model can outperform other baselines and each new component can bring significant improvement in terms of these three evaluation metrics. In addition, we can observe that the overall performance from the interpolation experiment is slightly worse than the extrapolation over-time experiment. This is because we only conduct interpolating tests in a single-crack experiment and use the beginning and end of crack data as training. It causes ML models to have difficulty capturing the complete dynamics of the crack without adding additional complete sequences of crack data (similar to extrapolating experiments' settings).

We also show the details of temporal analysis and visual results for this interpolation experiment in the supplementary file. We almost can obtain a similar conclusion as quantitative analysis. Our proposed method can achieve

promising reconstruction performance in this interpolation condition.

5.3. Fracture \rightarrow Fracture

This section represents the experimental results with Fracture \rightarrow Fracture, which includes extrapolation over the sample and over time. The setting of these experiments is the same with Cauchy features \rightarrow Fracture except the inputs are fracture damage.

5.3.1. Extrapolation Over Sample

Table 3 gives the RMSE, SSIM, and WFE of all the networks. From the results, we can see the improvement of the network with different regularization terms. When considering solely the implementation of physical regularization, the HOSSnet-F model does not exhibit a notable improvement in performance as compared to the CNN-LSTM model. With all the regularization terms, our proposed HOSSnet method still yields the lowest RMSE and WFE and the highest SSIM. The examples of the predicted fracture from HOSSNet at different time steps are shown in Figure 5. Compared to the scenario that uses Cauchy stress as the input, the network performs better when the input is the fracture because both input and output have the same properties. However, the damage is harder to obtain in the survey which makes this scenario harder to implement in the real world.

Table 3: Reconstruction performance (measured by RMSE, SSIM, and WFE) of Fracture \rightarrow Fracture’s experiment on the extrapolating over the sample (upper), extrapolating over time tests (middle), interpolating (lower) respectively.

Experiment	Method	RMSE↓	SSIM↑	WFE↓
Over Sample	HRU	0.029	0.976	0.124
	CNN-LSTM	0.026	0.985	0.058
	HOSSnet-F	0.023	0.986	0.074
	HOSSnet	0.013	0.993	0.045
Over Time	HRU	0.010	0.992	0.051
	CNN-LSTM	0.008	0.996	0.051
	HOSSnet-F	0.007	0.998	0.031
	HOSSnet	0.006	0.999	0.030

5.3.2. Extrapolation Over Time

According to the results presented in Table 3, the HOSSNet demonstrates the most superior performance. This is attributed to the fact that both the training and testing phases are carried out at distinct temporal intervals within the same crack. Consequently, the HOSSNet prediction exhibits the highest SSIM of 0.999 compared to other scenarios. Nonetheless, it is worth noting that a distinct network must be trained for each crack to be applied to diverse fractures, leading to increased computational expenses for this scenario.

6. Conclusion

In this paper, we develop a new data-driven method HOSSnet that integrates a series of physics regulations: optical flow, and positive direction to achieve fracture reconstruction in spatial-temporal. We also introduce extra machine learning optimization approaches to further improve the reconstruction. Moreover, we come up with two different experiment settings: Cauchy \rightarrow Fracture and Fracture \rightarrow Fracture to show the robustness and applicability of our proposed HOSSnet model. Our experiments demonstrate the effectiveness of these proposed methods in improving fracture reconstruction in extrapolating and interpolating tests. Furthermore, we also will propose new extensions by incorporating the underlying physical relationships (e.g. underlying partial differential equation(PDE) into the proposed model to further improve the reconstruction performance and evaluate our proposed HOSSnet method in larger micro-crack regions.

Acknowledgments

This work was funded by the Los Alamos National Laboratory (LANL) - Laboratory Directed Research and Development program under project number 20210542MFR.

References

- [1] Z. P. Bazant, J. Planas, *Fracture and size effect in concrete and other quasibrittle materials*, Routledge, 2019.
- [2] P.-E. Petersson, *Crack growth and development of fracture zones in plain concrete and similar materials*, Technical Report, Lund Inst. of Tech.(Sweden). Div. of Building Materials, 1981.
- [3] Z. Brooks, *Fracture process zone: Microstructure and nanomechanics in quasi-brittle materials*, Ph.D. thesis, Massachusetts Institute of Technology, 2013.
- [4] V. Veselý, L. Routil, Z. Keršner, *Structural geometry, fracture process zone and fracture energy*, *Proceedings of Fracture Mechanics of Concrete and Concrete Structures (Proc. FraMCoS-6)*, Al. Carpinteri, P. Gambarova, G. Ferro, G. Plizzari (eds.), Catania, Italy, Taylor & Francis/Balkema 1 (2007) 111–118.
- [5] S. W. Freiman, J. J. Mecholsky Jr, *The fracture of brittle materials: testing and analysis*, John Wiley & Sons, 2019.
- [6] J. Lamon, *Brittle fracture and damage of brittle materials and composites: statistical-probabilistic approaches*, Elsevier, 2016.
- [7] J. R. Rice, et al., *Mathematical analysis in the mechanics of fracture*, *Fracture: an advanced treatise 2* (1968) 191–311.
- [8] J. R. Rice, R. Thomson, *Ductile versus brittle behaviour of crystals*, *The Philosophical Magazine: A Journal of Theoretical Experimental and Applied Physics* 29 (1974) 73–97.
- [9] J. Hutchinson, *Plastic stress and strain fields at a crack tip*, *Journal of the Mechanics and Physics of Solids* 16 (1968) 337–342.
- [10] J. Hutchinson, *Singular behaviour at the end of a tensile crack in a hardening material*, *Journal of the Mechanics and Physics of Solids* 16 (1968) 13–31.
- [11] J. W. Hutchinson, Z. Suo, *Mixed mode cracking in layered materials*, *Advances in applied mechanics* 29 (1991) 63–191.
- [12] X.-P. Xu, A. Needleman, *Numerical simulations of fast crack growth in brittle solids*, *Journal of the Mechanics and Physics of Solids* 42 (1994) 1397–1434.
- [13] F. Z. Li, C. F. Shih, A. Needleman, *A comparison of methods for calculating energy release rates*, *Engineering fracture mechanics* 21 (1985) 405–421.
- [14] M. J. Buehler, F. F. Abraham, H. Gao, *Hyperelasticity governs dynamic fracture at a critical length scale*, *Nature* 426 (2003) 141–146.
- [15] K. Ravi-Chandar, B. Yang, *On the role of microcracks in the dynamic fracture of brittle materials*, *Journal of the Mechanics and Physics of Solids* 45 (1997) 535–563.
- [16] J. Desroches, E. Detournay, B. Lenoach, P. Papanastasiou, J. R. A. Pearson, M. Thiercelin, A. Cheng, *The crack tip region in hydraulic fracturing*, *Proceedings of the Royal Society of London. Series A: Mathematical and Physical Sciences* 447 (1994) 39–48.
- [17] A. Hillerborg, M. Modéer, P.-E. Petersson, *Analysis of crack formation and crack growth in concrete by means of fracture mechanics and finite elements*, *Cement and concrete research* 6 (1976) 773–781.
- [18] E. Knight, E. Rougier, Z. Lei, A. Munjiza, *User’s manual for Los Alamos National Laboratory hybrid optimization software suite (HOSS)-educational version*, Technical Report, Technical Report LA-UR-16-23118, Los Alamos National Laboratory, 2016.
- [19] V. Badrinarayanan, A. Kendall, R. Cipolla, *Segnet: A deep convolutional encoder-decoder architecture for image segmentation*, *IEEE transactions on pattern analysis and machine intelligence* 39 (2017) 2481–2495.
- [20] L.-C. Chen, Y. Zhu, G. Papandreou, F. Schroff, H. Adam, *Encoder-decoder with atrous separable convolution for semantic image segmentation*, in: *Proceedings of the European conference on computer vision (ECCV)*, 2018, pp. 801–818.
- [21] H. Yang, C. Huang, L. Wang, X. Luo, *An improved encoder–decoder network for ore image segmentation*, *IEEE Sensors Journal* 21 (2020) 11469–11475.
- [22] I. Häggström, C. R. Schmidlein, G. Campanella, T. J. Fuchs, *Deepnet: A deep encoder–decoder network for directly solving the pet image reconstruction inverse problem*, *Medical image analysis* 54 (2019) 253–262.
- [23] J. Montalt-Tordera, V. Muthurangu, A. Hauptmann, J. A. Steeden, *Machine learning in magnetic resonance imaging: image reconstruction*, *Physica Medica* 83 (2021) 79–87.
- [24] D. J. Lin, P. M. Johnson, F. Knoll, Y. W. Lui, *Artificial intelligence for MR image reconstruction: an overview for clinicians*, *Journal of Magnetic Resonance Imaging* 53 (2021) 1015–1028.
- [25] J. S. Read, X. Jia, J. Willard, A. P. Appling, J. A. Zwart, S. K. Oliver, A. Karpatne, G. J. Hansen, P. C. Hanson, W. Watkins, et al., *Process-guided deep learning predictions of lake water temperature*, *Water Resources Research* 55 (2019) 9173–9190.
- [26] R. Thavarajah, X. Zhai, Z. Ma, D. Castineira, *Fast modeling and understanding fluid dynamics systems with encoder–decoder networks*, *Machine Learning: Science and Technology* 2 (2021) 025022.
- [27] Z. Li, N. Kovachki, K. Azizzadenesheli, B. Liu, K. Bhattacharya, A. Stuart, A. Anandkumar, *Fourier neural operator for parametric partial differential equations*, arXiv preprint arXiv:2010.08895 (2020).
- [28] B. Li, H. Wang, X. Yang, Y. Lin, *Solving seismic wave equations on variable velocity models with fourier neural operator*, arXiv preprint arXiv:2209.12340 (2022).
- [29] G. Wen, Z. Li, K. Azizzadenesheli, A. Anandkumar, S. M. Benson, *U-fno—an enhanced fourier neural operator-based deep-learning model for multiphase flow*, *Advances in Water Resources* 163 (2022) 104180.
- [30] F. Kratzert, et al., *Toward improved predictions in ungauged basins: Exploiting the power of machine learning*, *WRR* (2019).
- [31] X. Jia, J. Willard, A. Karpatne, J. Reed, J. Zwart, M. Steinbach, V. Kumar, *Physics guided rns for modeling dynamical systems: A case study in simulating lake temperature profiles*, in: *Proceedings of the 2017 SIAM International Conference on Data Mining*, SIAM, 2019.
- [32] B. A. Moore, E. Rougier, D. O’Malley, G. Srinivasan, A. Hunter, H. Viswanathan, *Predictive modeling of dynamic fracture growth in brittle materials with machine learning*, *Computational Materials Science* 148 (2018) 46–53.
- [33] G. Srinivasan, J. D. Hyman, D. A. Osthus, B. A. Moore, D. O’Malley, S. Karra, E. Rougier, A. A. Hagberg, A. Hunter, H. S. Viswanathan, *Quantifying topological uncertainty in fractured systems using graph theory and machine learning*, *Scientific reports* 8 (2018) 11665.
- [34] A. Hunter, B. A. Moore, M. Mudunuru, V. Chau, R. Tchoua, C. Nyshadham, S. Karra, D. O’Malley, E. Rougier, H. Viswanathan, et al., *Reduced-order modeling through machine learning and graph-theoretic approaches for brittle fracture applications*, *Computational Materials Science* 157 (2019) 87–98.
- [35] M. Schwarzer, B. Rogan, Y. Ruan, Z. Song, D. Y. Lee, A. G. Percus, V. T. Chau, B. A. Moore, E. Rougier, H. S. Viswanathan, et al., *Learning to fail: Predicting fracture evolution in brittle material models using recurrent graph convolutional neural networks*, *Computational Materials Science* 162 (2019) 322–332.

- [36] R. L. Barkau, UNET: One-dimensional unsteady flow through a full network of open channels. User's manual, Technical Report, Hydrologic Engineering Center Davis CA, 1996.
- [37] S. Feng, X. Zhang, B. Wohlberg, N. P. Symons, Y. Lin, Connect the dots: In situ 4-d seismic monitoring of co 2 storage with spatio-temporal cnns, *IEEE Transactions on Geoscience and Remote Sensing* 60 (2021) 1–16.
- [38] Z. Moshe, et al., Hydronets: Leveraging river structure for hydrologic modeling (2020).
- [39] S. Chen, et al., Heterogeneous stream-reservoir graph networks with data assimilation, in: ICDM, 2021.
- [40] K. Fukami, K. Fukagata, K. Taira, Super-resolution reconstruction of turbulent flows with machine learning, *Journal of Fluid Mechanics* 870 (2019) 106–120.
- [41] B. Liu, J. Tang, H. Huang, X.-Y. Lu, Deep learning methods for super-resolution reconstruction of turbulent flows, *Physics of Fluids* 32 (2020) 025105.
- [42] Z. Deng, C. He, Y. Liu, K. C. Kim, Super-resolution reconstruction of turbulent velocity fields using a generative adversarial network-based artificial intelligence framework, *Physics of Fluids* 31 (2019) 125111.
- [43] X. Wang, K. Yu, S. Wu, J. Gu, Y. Liu, C. Dong, Y. Qiao, C. Change Loy, Esrgan: Enhanced super-resolution generative adversarial networks, in: *ECCV Workshops*, 2018.
- [44] R. Perera, D. Guzzetti, V. Agrawal, Graph neural networks for simulating crack coalescence and propagation in brittle materials, *Computer Methods in Applied Mechanics and Engineering* 395 (2022) 115021.
- [45] J. Willard, X. Jia, S. Xu, M. Steinbach, V. Kumar, Integrating physics-based modeling with machine learning: A survey, *arXiv preprint arXiv:2003.04919* (2020).
- [46] S. Cuomo, V. S. Di Cola, F. Giampaolo, G. Rozza, M. Raissi, F. Piccialli, Scientific machine learning through physics-informed neural networks: where we are and what's next, *Journal of Scientific Computing* 92 (2022) 88.
- [47] A. Karpatne, W. Watkins, J. Read, V. Kumar, Physics-guided neural networks (pgnn): An application in lake temperature modeling, *arXiv preprint arXiv:1710.11431* (2017).
- [48] A. Kahana, T. Eli, D. Shai, G. Dan, Obstacle segmentation based on the wave equation and deep learning, *Journal of Computational Physics* 413 (2020) 109458.
- [49] Wikipedia contributors, Rectifier (neural networks) — Wikipedia, the free encyclopedia, 2023. URL: [https://en.wikipedia.org/w/index.php?title=Rectifier_\(neural_networks\)&oldid=1132964988](https://en.wikipedia.org/w/index.php?title=Rectifier_(neural_networks)&oldid=1132964988), [Online; accessed 5-March-2023].
- [50] K. O'Shea, R. Nash, An introduction to convolutional neural networks, *arXiv preprint arXiv:1511.08458* (2015).
- [51] S. Ioffe, C. Szegedy, Batch normalization: Accelerating deep network training by reducing internal covariate shift, in: *International conference on machine learning*, PMLR, 2015, pp. 448–456.
- [52] K. He, X. Zhang, S. Ren, J. Sun, Delving deep into rectifiers: Surpassing human-level performance on imagenet classification, in: *Proceedings of the IEEE international conference on computer vision*, 2015, pp. 1026–1034.
- [53] S. Hochreiter, J. Schmidhuber, Long short-term memory, *Neural Computation* 9 (1997) 1735–1780.
- [54] B. K. Horn, B. G. Schunck, Determining optical flow, *Artificial intelligence* 17 (1981) 185–203.
- [55] K. Simonyan, A. Zisserman, Very deep convolutional networks for large-scale image recognition, *arXiv preprint arXiv:1409.1556* (2014).
- [56] Z. Wang, A. C. Bovik, H. R. Sheikh, E. P. Simoncelli, Image quality assessment: from error visibility to structural similarity, *IEEE transactions on image processing* 13 (2004) 600–612.
- [57] D. P. Kingma, J. Ba, Adam: A method for stochastic optimization, *arXiv preprint arXiv:1412.6980* (2014).

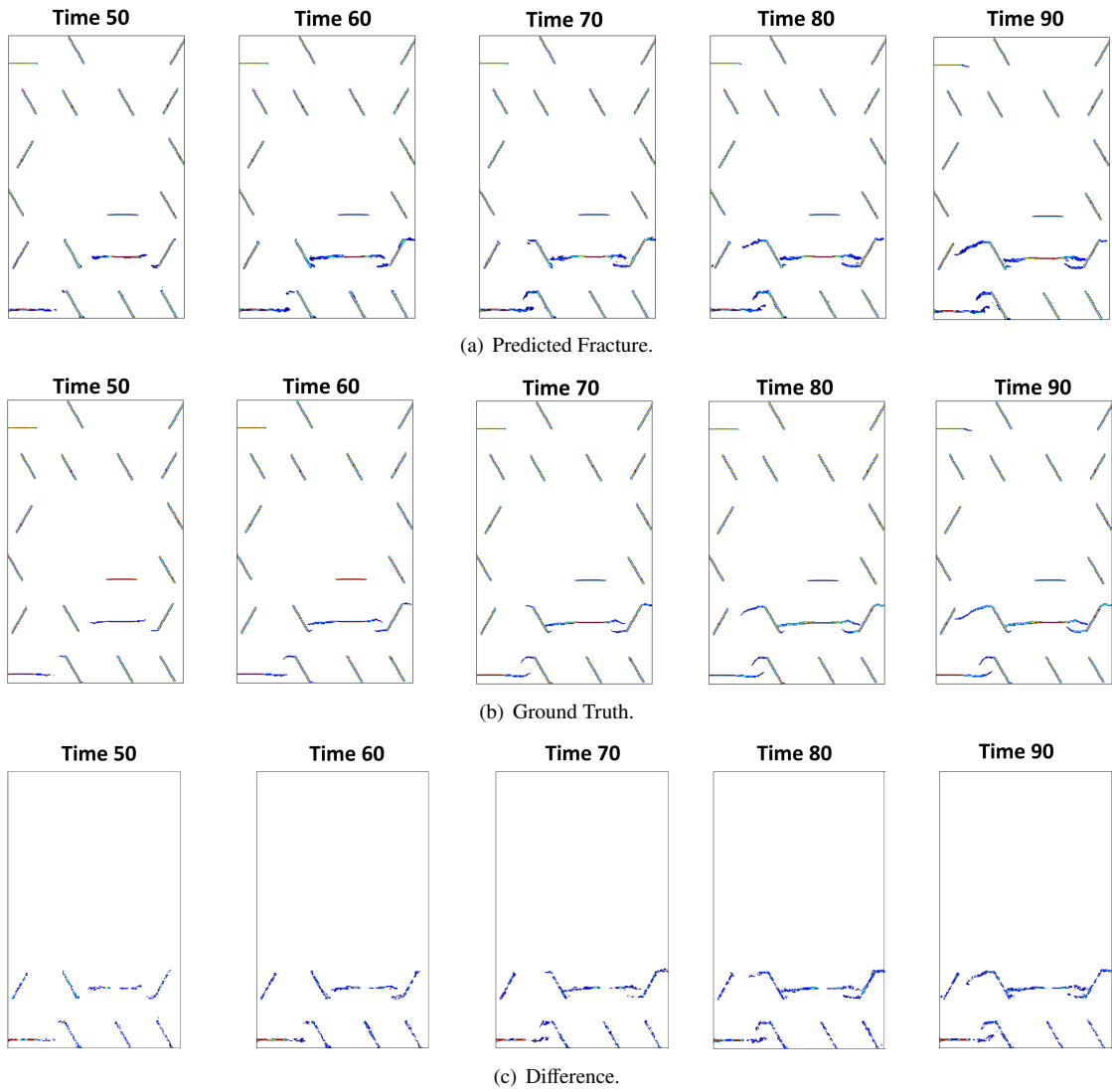


Fig. 4: Reconstructed fracture images by HOSSnet Model (top), real fracture images (middle), and difference (bottom) between reconstructed fracture and real fracture from the 1st to the 50th time steps (interval is 10 time steps) in the Cauchy→Fracture over sample scenario.

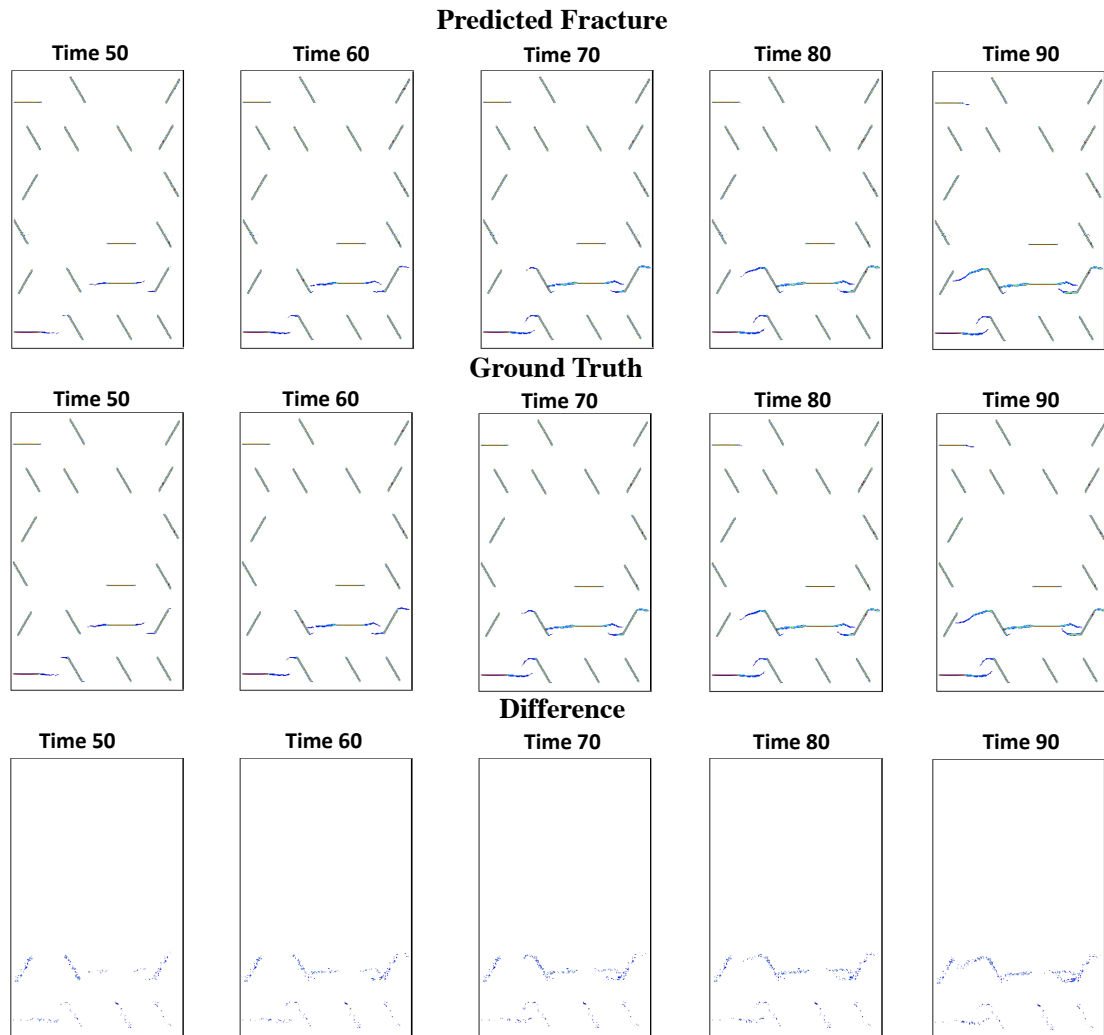


Fig. 5: Reconstructed fracture images by HOSSNet Model and real fracture images from the 1st to the 50th time steps (interval is 10-time steps) in the Fracture→Fracture over sample scenario.